Stochastic daily rainfall generation on tropical islands with complex topography

Lionel Benoit[1,2,5], Lydie Sichoix[2], Alison D. Nugent[3], Matthew P. Lucas[4], Thomas W. Giambelluca[1]

[1]Water Resources Research Center, University of Hawaiʻi at Mānoa, 96822 Honolulu, Hawaiʻi, USA
[2]GePaSud Laboratory, University of French Polynesia, 98702 Faaʻa - Tahiti, French Polynesia
[3]Department of Atmospheric Sciences, School of Ocean and Earth Science and Technology, University of Hawaiʻi at Mānoa, 96822 Honolulu, Hawaiʻi, USA
[4]Department of Geography, University of Hawaiʻi at Mānoa, 96822 Honolulu, Hawaiʻi, USA
[5]Now at Biostatistics and Spatial Processes (BioSP), INRAE, 84914 Avignon Cedex 9, France

Correspondence to: Lionel Benoit (benoitlionel2@gmail.com)

Abstract. Stochastic rainfall generators are probabilistic models of rainfall space-time behavior. During parameterization and calibration, they allow the identification and quantification of the main modes of rainfall variability. Hence, stochastic rainfall models can be regarded as probabilistic conceptual models of rainfall dynamics.

As with most conceptual models in Earth Sciences, the performance of stochastic rainfall models strongly relies on their adequacy in representing the rain process at hand. On tropical islands with high elevation topography, orographic rain enhancement challenges most existing stochastic models because it creates localized precipitations with strong spatial gradients, which break down the stationarity of rain statistics.

To allow for stochastic rainfall modeling on tropical islands, despite non-stationarity of rain statistics, we propose a new stochastic daily multi-site rainfall generator specifically for areas with significant orographic effects. Our model relies on a preliminary classification of daily rain patterns into rain types based on rainfall space and intensity statistics, and sheds new light on rainfall variability at the island scale. Within each rain type, the distribution of rainfall through the island is modeled by combining a non-parametric resampling of past analogs of a latent field describing the spatial distribution of rainfall, and a parametric Gamma transform function describing rain intensity.

When applied to the stochastic simulation of rainfall on the islands of Oʻahu (Hawaiʻi, United States of America) and Tahiti (French Polynesia) in the tropical Pacific, the proposed model demonstrates good skills in jointly simulating site-specific and island-scale rain statistics. Hence, it provides a new tool for stochastic impact studies in tropical islands, in particular for watershed water resources management.

1 Introduction

Stochastic rainfall generators are probabilistic tools aiming at simulating synthetic rainfall that mimic as closely as possible the statistical signature of rain observations [*Richardson*, 1981] [*Wilks and Wilby*, 1999] [*Ailliot et al.*, 2015]. More specifically, stochastic rainfall modeling consists of statistical learning (i.e., inference) of the joint space-time probability

32 density function (pdf) of rainfall at all sites and times of interest, and sampling this pdf to efficiently generate synthetic rainfall.

33 The ability of stochastic rainfall generators to emulate long and realistic rainfall sequences makes them an appropriate tool for

34 the simulation of design storms [*Niemi et al.*, 2016]. Simulated rainfall can then be used as inputs for impact models assessing

35 the effects of rainfall on different environmental processes including hydrology [*Paschalis et al.*, 2014], water resources

36 [*Cappelaere et al.*, 2020], geomorphology [*Peleg et al.*, 2020], and agronomy [*Mavromatis and Hansen*, 2001]. The

37 probabilistic approach followed by stochastic rainfall generators enables a comprehensive study of rainfall variability and, in

38 turn, the assessment of uncertainty propagation along the whole modeling chain [*Gabellani et al.*, 2007]. This makes stochastic

39 rainfall generation a key tool for management of rain-induced risk, in particular, for flood [*Caseri et al.*, 2016] and drought

40 risks [*Supit et al.*, 2012]. In addition, the focus of stochastic rainfall models on the statistical signature of rainfall creates new

41 ways to characterize rainfall space-time behavior [*Marra and Morin*, 2018], and assess the impact of rainfall variability on the

42 hydrosphere [*Morin et al.*, 2019]. Finally, when conditioned to climate model outputs, stochastic rainfall generation can be

43 used for the downscaling of future precipitation projections [*Maraun et al.*, 2010], resulting in local-scale and high-resolution

44 scenarios of the possible evolution of rainfall in the context of climate change [*Jha et al.*, 2014] [*Volosciuk et al.*, 2017].

45 To enable fast and computationally efficient simulations, and thereby allow for investigation of rainfall variability

46 and associated uncertainty through the simulation of large ensembles, stochastic rainfall generators adopt an empirical

47 approach that bypasses the detailed physical modeling of rain generation processes [*Bauer et al.*, 2015]. To avoid the pitfall of

48 physically unrealistic simulations, stochastic rainfall models embed a significant part of our conceptual knowledge about

49 rainfall behavior in their parameterization (i.e., they implement statistical relationships that reflect as closely as possible the

50 physical processes at work). However, rainfall properties [*Krajewski et al.*, 2003] and, in turn, the performance of stochastic

51 rainfall generators [*Breinl et al.*, 2017] [*Vu et al.*, 2018] strongly depend on the climate of the area of interest. Hence, different

52 models have been proposed for different climates with each model focusing on a specific aspect of rainfall, for instance: rainfall

53 seasonality in monsoonal climates [*Greene et al.*, 2011]; rainfall spatial-temporal correlation in temperate climates [*Paschalis

54 et al.*, 2013]; or rainfall occurrence and extreme intensities in arid regions [*Wilcox et al.*, 2021].

55 On high tropical islands, or islands with high elevations and significant topography, rainfall is strongly location

56 dependent due to complex interactions between atmospheric circulation and island topography, which trigger different

57 mechanisms of orographic rain enhancement [*Foresti and Pozdnoukhov*, 2012] [*Houze*, 2012]. At monthly to annual scales,

58 the effect of orographic lifting of relatively steady trade winds generates well defined rain patterns [*Lyons*, 1982]. In these

59 patterns, highlands are usually wetter than lowlands, windward slopes wetter than leeward sides, and in case of successive

60 mountain ridges the first to be reached by the wet air masses is the wettest [*Giambelluca et al.*, 2013] [*Laurent et al.*, 2019].

61 To this first order quasi-static picture is added the important variability of daily rainfall patterns associated with processes

62 ranging from synoptic-scale disturbances [*Hopuare et al.*, 2018] [*Longman et al.*, 2021] to large-scale atmospheric circulations

63 [*Hopuare et al.*, 2015] [*Frazier et al.*, 2018] [*Brown et al.*, 2020]. Large deviations from the long term rainfall patterns are

64 thus observed, and usually dry leeward slopes can become the wettest part of the island, for example during Kona storms

65 (seasonal cyclones) in the Hawai'i archipelago [*Caruso and Businger*, 2006].

Orographic effects lead to non-stationary (i.e., non-homogeneous) rain statistics in both space and time, which challenges most existing stochastic rainfall models [*Nerini et al.*, 2017]. In the context of high tropical islands, the first difficulty arises from the long term patterns of orographic rain enhancement that create non-stationarities in space. Rainfall generators must therefore account not only for the correlation between locations [*Leblois and Creutin*, 2013] [*Paschalis et al.*, 2013], but also for the location of the rain within the island. When orographic effects are directly related to topography, Generalized Linear Models (GLMs) have been leveraged to account for spatial rain patterns by linking model parameters to local topographic information such as altitude or slope aspect [*Ambrosino et al.*, 2014] [*Chandler*, 2020]. In tropical islands however, the complexity of the rain-topography relationships (e.g., successive mountain ridges becoming drier at similar altitude) hinder the direct regression of model parameters on topographic data. An interesting option to overcome the non-uniqueness of topography-rainfall relationships is to interpolate the parameters of the rainfall model in space in order to let data inform non-stationarity [*Kleiber et al.*, 2012] [*Bennett et al.*, 2018]. This however increases model complexity, and therefore requires training datasets with high spatial resolution, which are not yet available in most target areas [*Benoit et al.*, 2021]. Finally, the difficulty of accounting for orographic effects in the context of high tropical islands is further increased by the temporal variability of rainfall patterns (e.g., wet leeward slopes during Kona storms), which calls for the development of models able to identify and capture the main modes of variability of orographic effects over time.

A rainfall generator compatible with marine tropical climates and complex rain-topography interactions encountered in tropical islands is, to the best of our knowledge, still missing in the toolbox of stochastic rainfall generators. To fill this gap, the present paper proposes a new rainfall model dedicated to high tropical islands with significant and complex topography, which aims to account for both the long-term quasi-static patterns of rain accumulation and the day-to-day fluctuations of the rainfall spatial distribution. Specifically, the goal is to develop a daily resolution multi-site stochastic rainfall generator able to simulate: (1) site specific rain occurrence, persistence, intensity and seasonality; (2) spatial patterns of daily rain accumulation; and (3) areal rain statistics at the island scale.

To achieve these objectives, the remainder of the article is structured as follows. Section 2 briefly reviews the main features of tropical island rainfall and describes our stochastic rainfall model. Section 3 illustrates the performance of the model for the island of Oʻahu (Hawaiʻi, USA) in the tropical Pacific, and a similar test study is repeated in supplementary material for the island of Tahiti (French Polynesia) to demonstrate the versatility of the model. Finally, section 4 discusses how the focus on orographic rain enhancement has influenced the design of the model and provides concluding remarks.

2 Data and methods

2.1 Rainfall features of interest

Because stochastic rainfall models are data-driven, their structure depends on the rain features one wants to reproduce in simulations. Hence, the identification of the main features of daily rainfall in high tropical islands is a prerequisite for the design of the present model. For illustration purposes, we focus throughout the main text on the island of Oʻahu, Hawaiʻi (lon

98 = 158°W, lat = 21.5°N, area = 1545 km^2, max altitude = 1220 m). The available rain gauge observation dataset consists of

99 daily records from a network of 86 rain gauges spread over the island (Fig. 1a), and covers a 20-year period 1991–2011. It

100 corresponds to a compilation of quality controlled and gap-filled daily observations [*Longman et al.*, 2018]. Gap-filling was

101 performed using the normal ratio method [*Paulhus and Kohler*, 1952], and only stations with less than 5% gap-filled data are

102 kept for this study in order to minimize the impact of gap-filling on our results. To contextualize the observed rain patterns,

103 several meteorological covariates (e.g., pressure, temperature, humidity and wind) are investigated at the island scale. We use

104 the ERA5 reanalysis dataset [*Hersbach et al.*, 2018] at 12:00 PM HST to inform these covariates and average the values of the

105 12 grid cells (pixel size = 0.25° x 0.25°) encompassing the island of Oʻahu.

106 Figure 1 displays the main features of rainfall over the island of Oʻahu. It shows the strong impact of trade wind

107 induced orographic rain enhancement on the spatial distribution of annual precipitation (Fig. 1a), with windward (northeast)

108 sides significantly wetter than leeward (southwest) ones, and highlands generally wetter than lowlands. Note some important

109 details of this annual rainfall pattern, for example that the rain maximum is observed leeward of the main crest of the Koʻolau

110 range, and that the Koʻolau mountains are significantly wetter than the Waiʻanae range despite higher elevation. In addition to

111 prevailing orographic rainfall triggered by the interactions of trade winds with island topography (east-northeasterly trade

112 winds blow more than 280 days per year over the Hawaiian archipelago [*Longman et al.*, 2015]), the island of Oʻahu also

113 experiences spatially widespread rain events, mostly triggered by regional atmospheric disturbances such as cold fronts

114 originating from mid-latitudes and Kona storms (seasonal cyclones) [*Longman et al.*, 2021]. These atmospheric disturbances

115 mostly occur during (boreal) winter, which corresponds to the local rainy season (spanning from October–March). They

116 represent the main source of precipitation for dry leeward locations and are responsible for the enhanced seasonality of rain

117 accumulation in these areas (Fig. 1a).

118 The diversity of rain generation mechanisms (e.g., orographic lifting, cold fronts, or Kona lows) coupled with the

119 steep island topography of volcanic origin result in a complex distribution of rainfall in space and time, which produces highly

120 variable island-scale rain statistics (i.e., statistics summarizing rain behavior throughout the island for a given day). Figure 1

121 b–d shows that at the scale of the island of Oʻahu, daily rainfall is strongly intermittent in space (only 3% of the days record

122 rain at all gauge locations, and half of the time at least 20% of the gauges measure no rain, Fig. 1b), highly skewed (island-

123 scale rain accumulation average < 2.25mm/day 50% of the time, but island-scale maximum accumulation

124 > 15mm/day 50% of the time and reaches 500 mm/day, Fig 1c), and strongly variable in space (coefficient of variation > 1.3

125 50% of the time, and > 2.9 10% of the time).

126
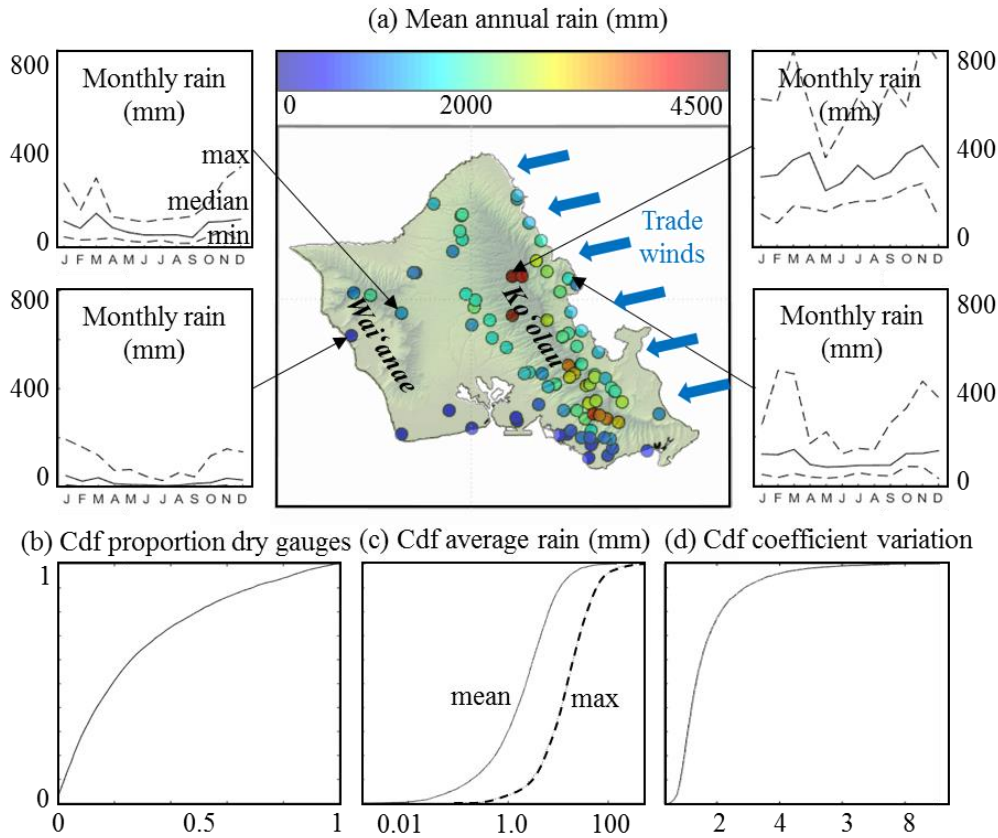
Figure 1: Main features of rainfall observed over the island of Oʻahu. (a) Mean annual rainfall (central panel) and seasonality of rain accumulation for four specific rain gauges (outer panels). (b) Cumulative distribution function (cdf) of the proportion of gauges measuring no rain for a given day. (c) Cdf of the mean and maximum daily rain accumulation computed over the whole observation network (abscissa is in log-scale). (d) Cdf of the coefficient of variation (i.e., standard deviation/mean) of daily rain accumulation throughout the rain gauge network.

2.2 Model description

2.2.1 Model overview

To model the statistical features of daily rainfall in tropical islands while accounting for the main mechanisms of orographic rain enhancement, in particular the variability of rainfall-topography relationships under the influence of changing atmospheric conditions, the proposed model splits rainfall behavior into three components: temporal variability, intensity (i.e., marginal distribution), and spatial distribution. Figure 2 summarizes the structure of the model, which is briefly introduced in the later part of this subsection, and will be discussed in detail in sections 2.2.2 to 2.2.4.

139
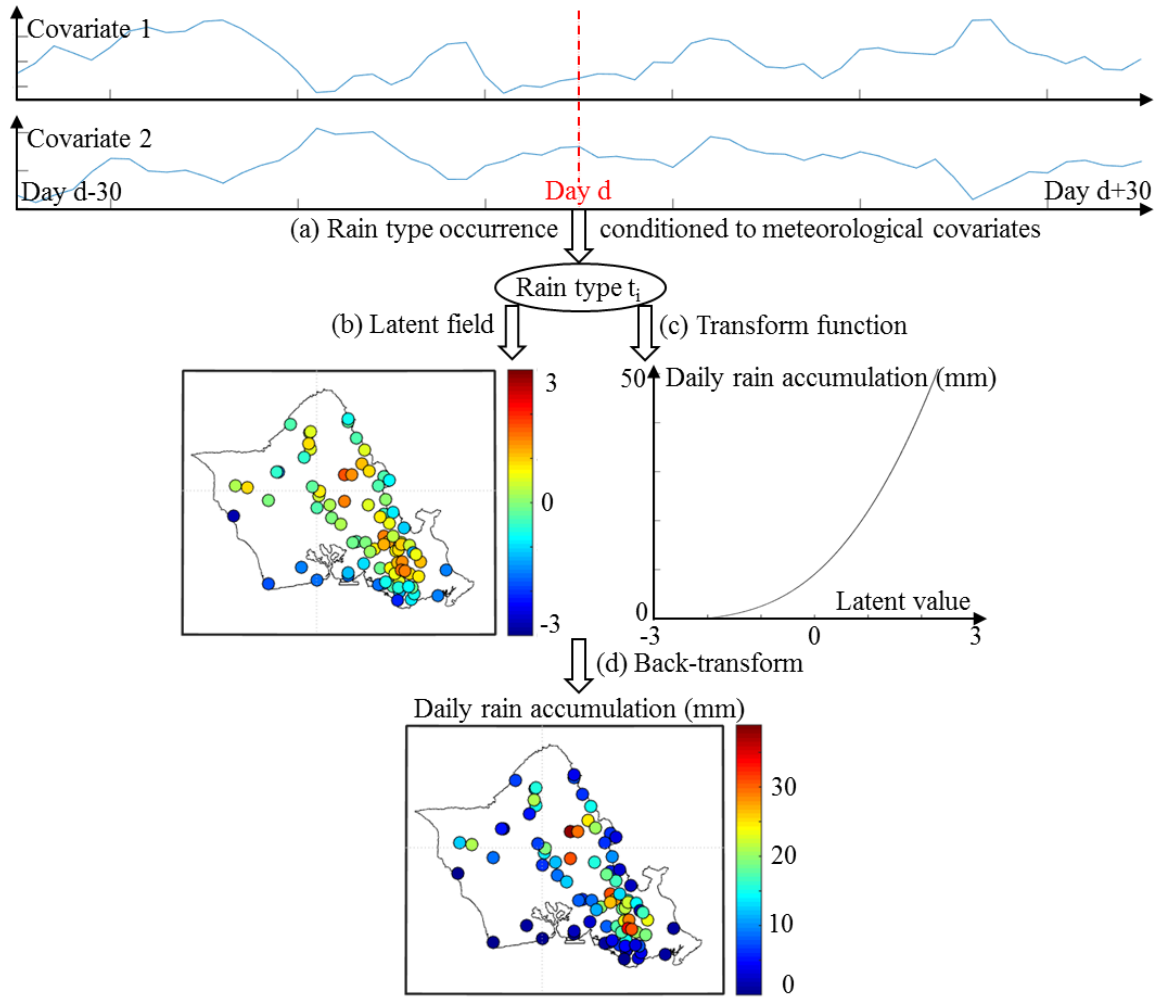
140 **Figure 2: Overview of the structure of the stochastic rainfall model.** (a) Meteorological covariates (here Geopotential at 950hPa and

141 Temperature difference between 950hPa and 700hPa) driving the occurrence of rain types, which summarize daily rain statistics. (b) Latent

142 field modeling of the spatial distribution of rainfall across the island. (c) Transform function linking latent values with actual rain

143 accumulations. (d) Back-transform combining (b) and (c) to obtain daily rain simulations.

144

145   The temporal variability of rain statistics and its relationships with the state of the atmosphere are modeled following

146 a rain typing approach (Fig. 2a) [*Ailliot et al.*, 2015] [*Benoit et al.*, 2018b]. In this framework, days with similar rain statistics

147 are first pooled together in a finite number of rain types, which represent summaries of island-scale daily rain statistics. Next,

148 rain type occurrence is modeled by a Markov chain describing how rain types transition to each other [*Bárdossy and Plate*,

149 1991] [*Wilby*, 1994]. To preserve climatological consistency and model the influence of atmospheric circulation on orographic

150 rain enhancement, rain type occurrence is conditioned to local meteorological covariates [*Benoit et al.*, 2020] making the

151 Markov chain non-homogeneous [*Hughes and Guttorp*, 1999] [*Vrac et al.*, 2007]. It is important to note here that we do not

use the widespread Hidden Markov Model (HMM) approach [*Ailliot et al.*, 2009] [*Greene et al.*, 2011] to introduce rain types in our stochastic rainfall model, but rather resort to a two-steps approach in which rain types are first determined by a direct classification of rain gauge observations, and subsequently a statistical rainfall model is built for each rain type. This choice has been motivated by the use of non-parametric methods to model the distribution of rainfall conditional to rain types, which prevents the formulation of the likelihood of the full statistical model and in turn the use of a HMM to model rain types.

Conditional to each rain type, the distribution of rain across the island is modeled following a meta-Gaussian approach (also referred to as trans-Gaussian or transformed Gaussian) [*Allard and Bourotte*, 2015] [*Baxevani and Lennartsson*, 2015] [*Papalexiou and Serinaldi*, 2020]. In this framework, a latent field with standardized Gaussian marginal distribution is non-linearly transformed to match the marginal distribution of daily rainfall across the island, and the spatial dependencies of the latent field are used to encode the spatial distribution of rainfall (Fig. 2b-c). The latent field is often assumed to follow a multivariate-Gaussian distribution, which allows for a parsimonious modeling of the spatial dependencies using geostatistics [*Lantuéjoul*, 2002], and in turn the spatial interpolation of rain gauge observations [*Benoit et al.*, 2018a]. In this study however, a careful investigation of inter-gauges spatial dependencies (Supplementary material 1) shows the inadequacy of the multivariate-Gaussian distribution to model the latent field. Instead, a non-parametric resampling of past analogs [*Gangopadhyay and Clark*, 2005] [*Yiou*, 2014] of the daily latent field is used to model spatial dependencies. Aside from the choice of the marginal distribution of the latent field (Gaussian vs. uniform), this model is comparable to the use of empirical spatial copulas [*Bárdossy and Pegram*, 2009] coupled with a parametric marginal distribution of non-zero rain accumulation. This approach has the advantage of faithfully reproducing the complex spatial distribution of rainfall due to orographic effects, but at the expense of the ability to spatial interpolation. The present model should therefore be regarded as a multi-site stochastic rainfall generator (and not a rain field generator), and the spatial interpolation of the simulated multi-site rainfall is kept out of the scope of this paper.

2.2.2 Meta-Gaussian representation of island-scale daily rainfall

Rain intensity and spatial distribution are modeled jointly following a meta-Gaussian approach (Fig. 2b-c). For a given day, the observed rain accumulations $R_{i=1 \dots N_T}$ across a network of N_T gauges are linked to their latent counterparts Z_i (which follow a standardized Gaussian marginal distribution, i.e., $Z \sim \mathcal{N}(0,1)$) through a non-linear transform function ψ. This transformation is performed by first assuming that non-zero rain accumulations observed throughout the island in a given day follow a Gamma distribution:

$$Z_i = \psi(R_i) = \Phi^{-1}\left(\frac{N_d}{N_T} + \frac{N_w}{N_T} \times Gamma(R_i; k, \theta)\right) \; if \; R_i > 0 \tag{1}$$

where N_d, N_w are the number of dry and wet gauges, Φ^{-1} is the inverse cumulative distribution function (cdf) of the univariate standardized Gaussian distribution, and $Gamma(R_i; k, \theta)$ is the cdf of the Gamma distribution with shape parameter $k > 0$ and scale parameter $\theta > 0$.

184   In many instances, gauges measuring no rain (i.e., $R_i=0$) represent a significant part of the network, which creates a

185   concentration of zero values in rain accumulation distribution, and prevents a correct Gaussian transform using the function of

186   Eq. (1). To circumvent this problem, the latent values corresponding to dry gauges are assigned based on the distance of the

187   dry gauges to the closest wet gauge, such as the marginal distribution of the latent values matches the left portion of a

188   standardized normal distribution. The idea behind this application-specific solution to deal with the spatial intermittence of

189   rainfall is that a location far from any wet gauge should remain dry even after combining the associated latent field with slightly

190   different parameters of the transform function (Eq. 1-2) during the simulation step (Sect. 2.3.3). In case of a gauge measuring

191   no-rain ($R_i = 0$), the corresponding latent value is given by:

192
$$Z_i = \psi(R_i) = \Phi^{-1}\left(\left(1 - \frac{Dw_i}{max_{j=1:N_d}(Dw_j)}\right) \times \frac{N_d}{N_T}\right) \; if \; R_i = 0 \tag{2}$$

193   where Dw_i is the distance of the gauge i observing no rain to the closest gauge measuring non-zero rain. This transformation

194   has the advantage of creating spatial patterns of censored latent values (i.e., corresponding to dry gauges) that are coherent

195   with the ones of non-censored latent values (i.e., corresponding to wet gauges), and create smooth transitions between wet and

196   dry domains.

197   Once latent values (Z_i) are derived from rain observations (R_i), the spatial distribution of rain across the island is

198   defined by the spatial distribution of the latent field [*Bárdossy and Pegram*, 2009], i.e., the joint cdf of Z_i. As mentioned in

199   section 2.1, the spatial distribution of daily rainfall in high tropical islands is complex and strongly non-stationary due to

200   orographic effects, which prevents the use of a simple parametric form (such as the multivariate Gaussian distribution used in

201   most meta-Gaussian models of precipitation [*Benoit et al.*, 2018a] [*Papalexiou and Serinaldi*, 2020]) for the spatial

202   dependencies. Hence, in the present case, the non-parametric resampling of past latent fields is used to simulate the spatial

203   distribution of rainfall [*Rüschendorf*, 2009].

2.2.3 Rain typing

205   Based on the above meta-Gaussian representation of daily rain fields, days with similar rain statistics are pooled into

206   rain types (Fig. 2a) using a non-supervised clustering applied on the six-dimensional feature-space defined by the following:

207   -   The three parameters of the transform function (ψ) (i.e., $p_0 = \frac{N_d}{N_T}$, k, θ), which inform the marginal distribution of daily

208   rainfall over the island.

209   -   The first three components of the Karhunen-Loève expansion [*Huang et al.*, 2001] of the latent field Z

210   (PC_1, PC_2, PC_3), which inform the spatial distribution of rainfall across the island.

211   Based on this feature-space $Y = (p_0, k, \theta, PC_1, PC_2, PC_3)^T$, the clustering is performed using a Gaussian Mixture

212   Model (GMM, [*Fraley and Raftery*, 2002]) which approximates the pdf of **Y** as a weighted sum of multivariate Normal

213   distributions:

214
$$p_Y(\mathbf{Y} = \mathbf{y}) = \sum_{l=1:N_C} b_l \times \mathcal{N}(\mathbf{y}|\,\boldsymbol{\mu}_l, \boldsymbol{\Sigma}_l) \tag{3}$$

where p_Y is the joint pdf of the random vector Y, N_C is number of components in the GMM, b_l is a weight assigned to the lth component, and $\boldsymbol{\mu}_l$ and $\boldsymbol{\Sigma}_l$ are the mean vector and covariance matrix of the multivariate normal distribution of the lth component. Here, the parameters embedded in the vector Y are assumed to be only slightly correlated and the covariance matrices ($\boldsymbol{\Sigma}_l$) are therefore assumed to be diagonal. The number of components of the GMM (N_C) is selected by minimization of the Bayesian Information Criterion (BIC [*Schwartz*, 1978]) estimated for different numbers of components in order to select a parsimonious classification (i.e., with as few rain types as possible) while properly fitting the pdf of Y (i.e., p_Y). Once the pdf p_Y is known, the probability that an observed vector $\boldsymbol{y}_{obs}$ belongs to the lth component C_l is given by:

$$p(\boldsymbol{y}_{obs} \in C_l) = \frac{b_l \times \mathcal{N}(\boldsymbol{y}_{obs}|\boldsymbol{\mu}_l,\boldsymbol{\Sigma}_l)}{\sum_{k=1}^{N_C} b_k \times \mathcal{N}(\boldsymbol{y}_{obs}|\boldsymbol{\mu}_k,\boldsymbol{\Sigma}_k)} . \tag{4}$$

And the classification is obtained by assigning each day (d_i) with a rain type (RT) that corresponds to the most probable mixture component:

$$RT(d_i) = max_{l \in 1..N_C}(p(\boldsymbol{y}_i \in C_l)). \tag{5}$$

2.2.4 Rain type occurrence

Once rain types have been defined based on rainfall statistical properties, their occurrence is conditioned to the vector $\boldsymbol{MC}_d$ of meteorological covariates observed at day d (Fig. 2a), and rain type occurrence is modeled by a non-homogeneous Markov Chain of order 1 [*Hughes and Guttorp*, 1999] [*Vrac et al.*, 2007]:

$$p(RT_d = j|RT_{d-1} = i, \boldsymbol{MC}_d) \propto \gamma_{ij} \exp\left(-\frac{1}{2}(\boldsymbol{MC}_d - \boldsymbol{\mu}_{ij})\boldsymbol{\Sigma}_{ij}^{-1}(\boldsymbol{MC}_d - \boldsymbol{\mu}_{ij})^T\right) \tag{6}$$

Where RT_d is the state of the Markov chain (i.e., the rain type) at day d, $p(RT_d = j|RT_{d-1} = i, \boldsymbol{MC}_d)$ is the probability to transition from rain type i to rain type j, $\boldsymbol{\Sigma}_{ij}$ and $\boldsymbol{\mu}_{ij}$ are the covariance matrix and the mean vector of the meteorological covariates when the transition from type i to type j occurs, and γ_{ij} is the baseline (i.e., long term average) probability of transition from type i to type j. This model allows the transition probability $p(RT_d = j|RT_{d-1} = i, \boldsymbol{MC}_d)$ to vary proportionally to the conditional density of $\boldsymbol{MC}_d$ given the transition, and conditions the occurrence of rain types to the state of the atmosphere characterized by the covariates.

2.3 Model implementation

2.3.1 Selection of meteorological covariates

The set of meteorological covariates used for the conditioning of the non-homogeneous Markov Chain must be chosen so that: (i) the covariates are only weakly correlated to each other, which ensures model parsimony (i.e., minimal redundancy between covariates); and (ii) the temporal variations of the covariates are correlated with variations in rain type occurrence (Supplementary Material 2), which indirectly informs the seasonality and interannual variability of rainfall patterns. Note that in the present framework, the conditioning to covariates (i.e., the non-homogeneous part of the Markov chain) is used to inform the low frequency fluctuations of rain type occurrence (seasonal to interannual time scales), with higher frequencies (weekly

to daily time scales) being informed by the baseline transition probabilities (γ_{ij}). Hence, meteorological covariates are aggregated at the monthly scale prior to use for the conditioning of the non-homogeneous Markov chain. The monthly-aggregated covariates inform monthly anomalies in atmospheric conditions and, in turn, the likelihood of rain types to occur during a given month.

In the present case, we selected the meteorological covariates according to our initial knowledge about rain generation mechanisms in high tropical islands, and their links with the state of the atmosphere [*Elison Timm et al.*, 2014] [*Réchou et al.*, 2019] [*Sanfilippo*, 2020]; this led to the following five covariates.

1) Geopotential height at 700 hPa ($m^2.s^{-2}$). This covariate is correlated with the presence of synoptic-scale weather systems at the vicinity of the island and identifies regional atmospheric disturbances.

2) Temperature difference between 950 hPa and 700 hPa (K). This covariate is correlated with the lower atmospheric instability and identifies days prone to shallow convection.

3) Specific humidity at 700 hPa ($kg.kg^{-1}$). This covariate informs the presence of humidity above the height of the trade wind inversion and is negatively correlated with the strength of the inversion and positively correlated with the potential for deep convection and cold rain.

4) Meridional and 5) longitudinal humidity fluxes at 950 hPa (i.e., specific humidity multiplied by the *u* (east-west) or *v* (north-south) components of the wind field, $m.s^{-1}.kg.kg^{-1}$). These covariates provide the amount of moisture crossing over the mountain barrier available for precipitation and are a proxy for orographic precipitation.

2.3.2 Model calibration

The model is calibrated from a training dataset made of *N* days of rain accumulation recorded by a network of N_T rain gauges (Fig. 1a). Data must be available for all stations and all days of the calibration period, and a preliminary gap-filling step is required in case of incomplete data [*Longman et al.*, 2018] [*Oriani et al.*, 2020]. Once a complete training dataset is available, the first step of model calibration consists of inferring the parameters of the transform function (ψ) for each day of the training period. This is performed by calculating the proportion of dry gauges and then estimating the parameters of the gamma distribution of the wet gauges using a maximum likelihood approach. Once the three parameters of ψ are known, this function can be inverted to derive the latent values at each gauge location.

After calibration of the transform function and derivation of the latent values for each day of the calibration dataset, days with similar rain statistics are pooled together by rain typing. The first three principal components of the latent field are preliminarily derived from the Karhunen-Loève transform of all latent values. Next, the parameters of the GMM are inferred using an expectation-minimization approach [*Fraley and Raftery*, 2002]. Finally, rain typing (i.e., clustering) is performed by assigning to each day the type that corresponds to the most probable component of the GMM.

After rain typing, the time series of observed rain types is analyzed in relation to observations of the meteorological covariates to calibrate the non-homogeneous Markov chain. The baseline transition matrix (γ_{ij}) is first estimated by counting

277 the transitions between each pair of rain types occurring during the calibration period and normalizing the result by the total

278 number of transitions. Next, the parameters of the mean vector ($\boldsymbol{\mu}_{ij}$) and the covariance matrix ($\boldsymbol{\Sigma}_{ij}$) used to make the Markov

279 chain non-homogeneous are estimated by the method of moments applied to covariates observations.

280   Conditional to each rain type, the joint distribution of the parameters of ψ is inferred by multivariate kernel density

281 estimation using a trivariate Gaussian kernel. The bandwidth of the kernel is selected following the Scott's rule [*Scott*, 1979]

282 [*Scott*, 2010], i.e., in the present case:

283
$$\sqrt{\boldsymbol{H}_{ii}} = N^{-\frac{1}{7}} \times \sigma_i \tag{7}$$

284 where $\boldsymbol{H}$ is the bandwidth matrix of the kernel, N the number of days in the calibration dataset, and σ_i the standard deviation

285 of the ith parameter (here i=1..3).

286   Finally, because the latent field is simulated using an analog approach (cf next sub-section for details), this part of the

287 model does not require formal inference.

2.3.3 Stochastic rainfall generation

289   After model calibration, stochastic rainfall generation is performed following the steps summarized in Fig. 2. Starting

290 from a time series of meteorological covariates, rain types are first simulated using the non-homogeneous Markov chain

291 described in Eq. (6). Next, conditional to this simulated rain type time series, the parameters of the transform function are

292 sampled from their joint distribution defined by Eq. (7). Subsequently, one realization of the latent field is simulated using an

293 analog approach [*Gangopadhyay and Clark*, 2005] [*Mezghani and Hingray*, 2009] [*Yiou*, 2014], i.e., by randomly picking the

294 latent field of a day belonging to the same rain type as the day to simulate from the calibration dataset. Finally, the simulated

295 rain field is obtained by back-transformation of the simulated latent field (Eq. 1–2) using the simulated parameters of the

296 transform function.

2.4 Model assessment

298   The ability of the model to identify climatologically relevant rain types is assessed qualitatively by applying rain

299 typing to the full study dataset of section 2.1 and scrutinizing the emergent spatial-temporal rainfall patterns for each type. The

300 resulting classification is subsequently interpreted in terms of rain generation processes by confronting rain types with co-

301 occurring meteorological covariates. However, in doing so, one should keep in mind that the rain typing procedure is fully

302 statistical and that the rain type description is based on emerging statistical patterns, not on physical modeling (e.g., using a

303 numerical weather model to reproduce the observed patterns).

304   When discussing rain types and their link to rain generation processes, special attention is paid to:

305 (1) The emergence of spatial patterns in relation with orographic effects;

306 (2) The seasonality of rain type occurrence in relation with the regional annual rain cycle;

(3) The relationship of rain types with the state of the atmosphere quantified by the set of climate covariates described in section 2.4 and used here at a daily resolution (i.e., not aggregated at the monthly scale as is the case for the conditioning of the non-homogeneous Markov chain).

After the assessment of the climatological realism of rain types, the ability of the model to stochastically generate rainfall is assessed using a leave-one-year-out cross-validation procedure. Data from one year are iteratively removed from the study dataset of section 2.1 and the stochastic model is calibrated using the remaining data (i.e., 19 years of data are used for model calibration). The model is fully recalibrated, which includes rain typing, inference of the transform function, and creation of a training dataset of latent fields. After model calibration, daily rainfall is simulated for each day of the target year, i.e., the year excluded from the calibration dataset. Fifty simulations are generated to assess the uncertainty associated with stochastic rainfall generation. The same procedure is repeated for each year of the study dataset, which leads to a 20-year long validation set made of 50 simulations for each gauge of the Oʻahu rain-monitoring network.

Simulated rainfall is compared to observations following a multi-criteria approach. First, simulation results are evaluated qualitatively by visual inspection of rainfall time series for the four target stations of Fig 1.a. Next, a quantitative assessment is performed using the following evaluation statistics:

(1) Site-specific rain statistics. The following statistics are considered: quantiles 10%, 50% and 90% of monthly rain accumulation to assess seasonality; annual rain accumulation to assess interannual variability; quantile-quantile (q-q) plot of the percentiles of daily rain accumulation to assess the probability distribution of daily rainfall; and q-q plot of the percentiles of wet-spell duration to assess rain persistence.

(2) Spatial patterns of rain distribution across the island. The following statistics are mapped to investigate the spatial distribution of rainfall: quantiles 10%, 30%, 50%, 70% and 90% of daily rain to assess how the probability distribution of rainfall varies in space.

(3) Areal rain statistics. Q-q plots of the percentiles of (i) the proportion of dry rain gauges, (ii) mean and (iii) max of daily rain, and (iv) the coefficient of variation of rain accumulation across the island to assess island-scale statistics.

3 Results

3.1 Rain types in Oʻahu

Figure 3 displays the 22 rain types identified for Oʻahu Island during the period 1991–2011. Although this number may seem high compared to the number of rain types inferred for mid-latitude continental climates (usually less than 10 types, see e.g. [*Vrac et al.*, 2007] [*Benoit et al.*, 2018b]), we believe that it reflects the tremendous variability of rainfall observed in the Hawaiʻi archipelago [*Giambelluca et al.*, 2013], which led Hawaiians to use more than one hundred different words to describe rainfall [*Akana and Gonzalez*, 2015]. In addition to the large number of rain types required to account for rainfall variability in tropical islands, one key attribute of the resulting classification is that although no information is given to the

classifier about geographical coordinates, time of occurrence, or meteorological covariates, the identified rain types display

well-defined patterns of spatial rain distribution (Fig. 3a), seasonality of occurrence (Fig. 3a), and correlation with the regional

state of the atmosphere (Supplementary Material 2).

341
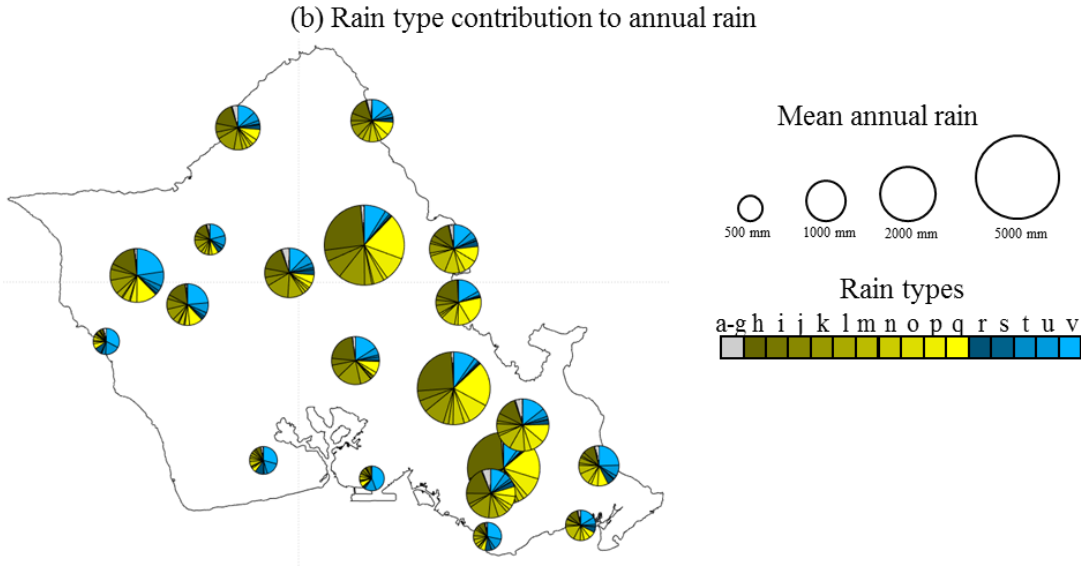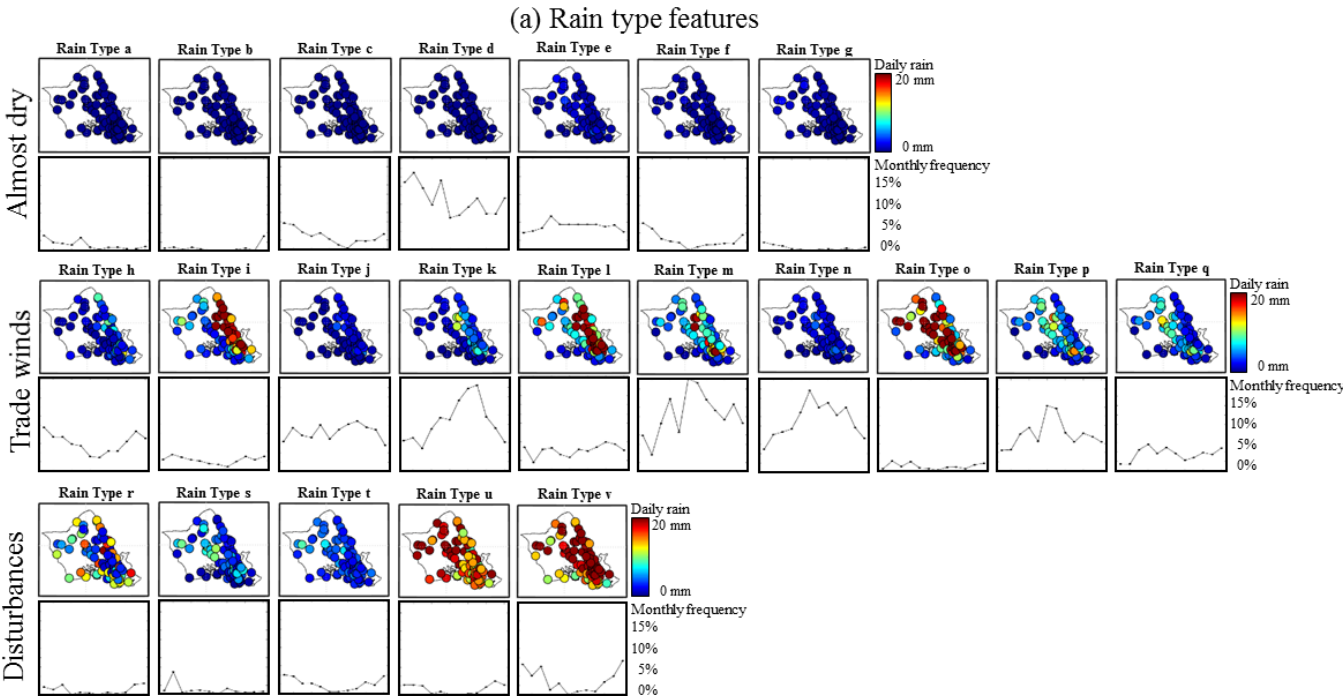
Figure 3: Rain types identified for the island of Oʻahu. (a) Spatial distribution of daily rain and frequency of occurrence of each rain type.

(b) Contribution of each rain type to the annual rain accumulation for a selection of 20 gauges spread throughout the island.

344

345   To better identify the main modes of rainfall variability over Oʻahu, rain types are pooled into three hyperclasses (H1-
346   3) that can be linked to the three main rain generation processes in the area (Fig. 3):

347   •   (H1) Almost dry days (Fig. 3, rain types a–g). During these days, most rain gauges report no rain, and no gauge
348   reports more than 5 mm/day on average. These types of weather conditions are associated with a stable atmosphere
349   and a low moisture flux (Fig. SM 2.1).

350   •   (H2) Trade wind days (Fig. 3, rain types h–q). This category displays well-defined spatial patterns of rain
351   accumulation caused by orographic lifting, and are associated with a stable atmosphere, a well-defined trade wind
352   inversion, and an important influx of moisture below the inversion layer under the influence of east-northeasterly
353   trade winds (Fig. SM 2.1). When scrutinizing inter-type variability within this category, note that the location of the
354   rain maximum shifts westward with increasing moisture flux, likely due to stronger trade winds causing an overshoot
355   of orographic rain enhancement whereby rain forms over the mountains but falls further downwind on the leeward
356   side [*Daly et al.*, 2017]. In addition, for similar wind conditions and, therefore, spatial patterns (compare for instance
357   types j, k and l), rain intensity is correlated to the instability of the atmosphere (Fig. SM 2.1).

358   •   (H3) Regional atmospheric disturbance days (Fig. 3, rain types r-v). These types display either unstructured (types r–
359   t) or relatively homogeneous (types u–v) spatial patterns of rain accumulation and are associated with low pressure,
360   unstable atmosphere, and absent (or weak) trade wind inversion. This allows high moisture content at high altitude
361   (Fig. SM 2.1). These rain types mostly occur during winter, i.e., the local rainy season. When scrutinizing inter-type
362   variability within this category, note that rain intensity increases with atmospheric instability and the presence of
363   humidity at high altitude, and that the spatial patterns tend to become more structured when the low-level moisture
364   influx increases (probably due to stronger and more uniform winds).

365   Hence, rain typing provides new insights on island-scale rain climatology (Fig. 3b). In particular, this step helps us
366   gain a better understanding of how different atmospheric conditions lead to different rain generation processes that, when
367   interacting with island topography, generate contrasting orographic effects. In the case of the island of Oʻahu, orographic rain
368   enhancement occurring during days influenced by trade winds is the main explanation for the high annual rain accumulations
369   in the Koʻolau mountains (up to 5000 mm annual rainfall), while widespread rainfall linked to regional atmospheric
370   disturbances is the main source of rain at leeward locations despite their relative temporal scarcity.

371

372   **3.2 Simulation of site-specific rainfall time series**

373   Figure 4 displays stochastic rainfall generation outputs for the four rain gauges of Fig 1.a which experience different
374   rainfall climatologies. Visual inspection of the simulated time series shows that our stochastic rainfall generator is able to
375   simulate synthetic rainfall that is almost indistinguishable from the observed one. The dry-wet ratio as well as the marginal
376   distribution of daily rain accumulation seem properly replicated, except for the dry leeward gauge (first row in Fig. 4) where
377   the 20-year maximum tends to be overestimated (see also Fig. 5.d). In terms of temporal variability, the simulated time series

378   properly capture the seasonal cycle visible for the two leeward gauges (rows 1-2 in Fig. 4), as well as the inter-annual variability

379   visible for the two coastal gauges (rows 1 and 4 in Fig. 4). Finally, the rainfall generator captures the relatively steady behavior

380   of the wet gauge located in the Ko'olau range (row 3 in Fig. 4).

381

382
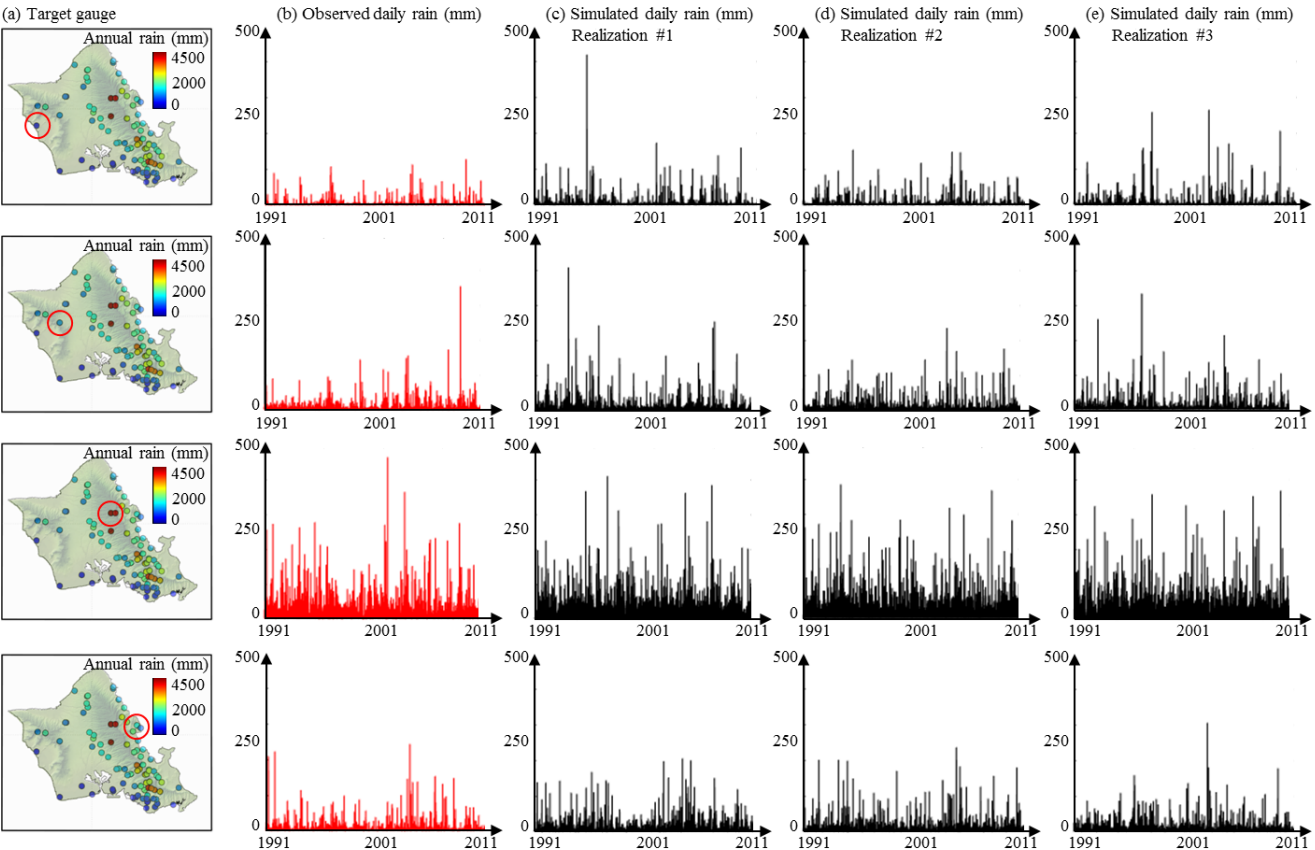
383   **Figure 4: Ability of the model to simulate realistic rainfall time series on O'ahu.** (a) Target locations. (b) Observed rainfall time series

384   for the period 1991-2011. (c-e) Simulated time series. For readability, only the three first realizations of the 50-member ensemble are

385   displayed.

386

387   **3.3 Simulation of site-specific rain statistics**

388   To complement the qualitative assessment of site-specific rainfall time series in Figure 4, Figure 5 investigates the

389   statistical features of the results of the cross-validation procedure (50 realizations are drawn) for the same four rain gauges.

390
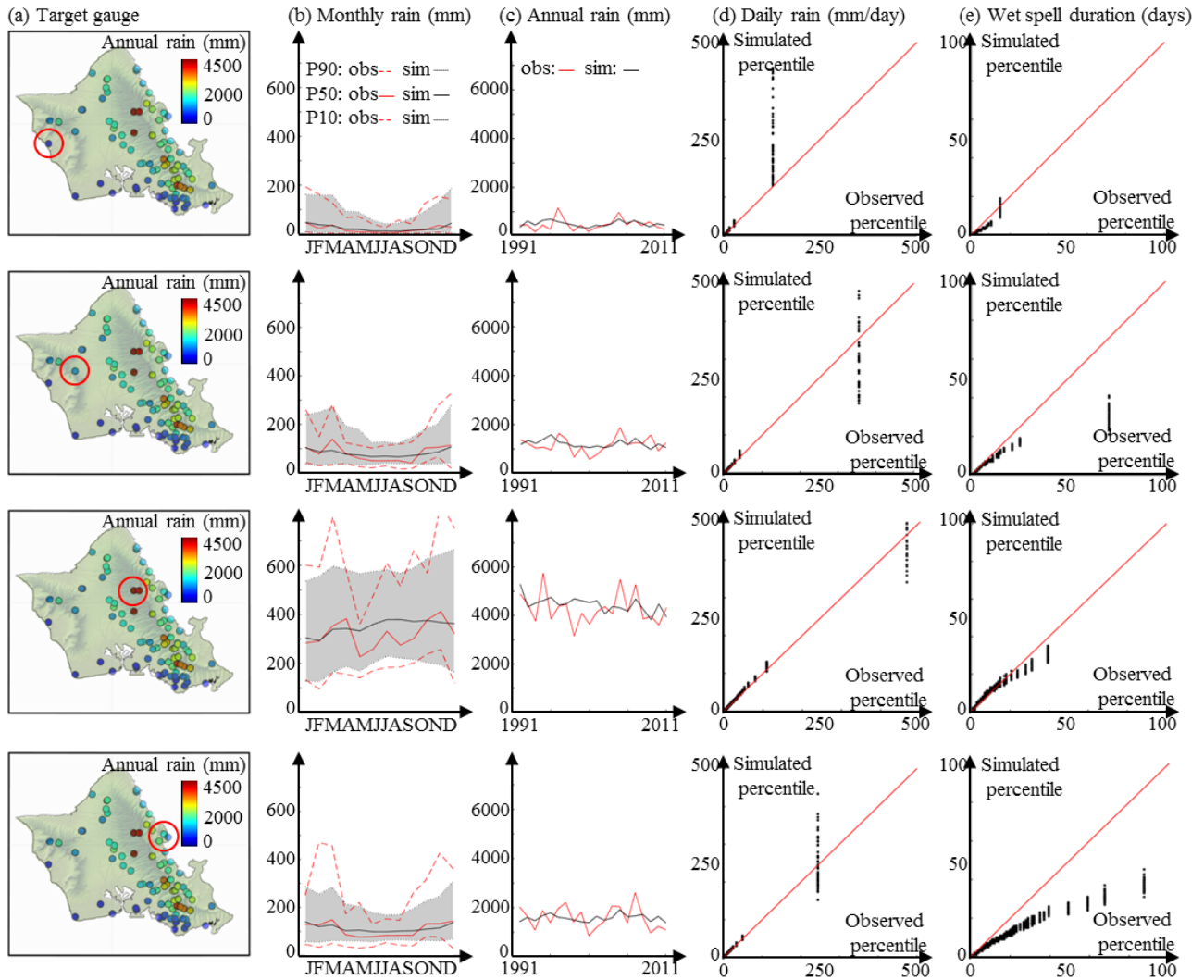
Figure 5: Ability of the model to simulate site-specific rain statistics on Oʻahu. (a) Target locations. (b) Observed (red) and simulated
(black) monthly rain accumulation. Dashed lines denote quantiles 10% and 90%, and solid lines denote the quantile 50%. In the case of
simulations (black), for readability, we report in the figure only the median of each quantile (10%, 50%, 90%) instead of 50 simulated
quantiles. The grey band between the dashed black lines denotes the interval Q10%-Q90% derived from simulations. (c) Observed (red) and
simulated (black) annual rain accumulation. In the case of simulations (black), for readability, we report in the figure only the median of the
50 simulations. (d) Q-q plot of daily rain percentiles. (e) Q-q plot of wet-spell duration percentiles. In (d-e) we display q-q plots between
one observation time series (abscissa) and 50 simulations (ordinates). Hence, black dots line up vertically in the q-q plots because for each
percentile, 50 simulations are compared to a single observation.

The results in Fig. 5 show that the proposed model correctly simulates rainfall seasonality (Fig. 5b) and interannual
variability (Fig. 5c). Note that simulations capture both the stronger seasonality at leeward locations (compared to windward

locations) as well as the near absence of seasonality at the wettest gauge located in Koʻolau Mountains (Fig. 5, third row). The interannual variability of rain accumulation is also properly simulated, in particular, at leeward locations where the impact of winter storms is the highest. These results suggest that the non-homogeneous Markov chain of order 1 conditioned to monthly-aggregated meteorological covariates adequately models the long-term variability of rain accumulation, and that the selected covariates properly capture rain type occurrence in a tropical marine climate.

However, rain persistence is slightly underestimated at some locations, especially for the high percentiles, i.e., long-lasting wet spells (Fig. 5e). This result exposes limitations in the use of the non-homogeneous Markov chain of order 1 for modeling weekly-scale temporal variability of rainfall. This may be explained by the fact that daily-scale and seasonal-scale rainfall fluctuations are informed, respectively, by the Markov chain of order 1 and conditioning to monthly-aggregated meteorological covariates, but that the weekly-scale is not explicitly included in the model. Although the resulting errors are of low magnitude, they should be kept in mind in case of applications requiring a precise estimation of rain persistence, for example crop models in semi-arid environments that can be found in some leeward areas of the target islands.

The simulations properly reproduce site-specific marginal distributions of daily rain accumulation (Fig. 5d), except for the driest gauge (top row in Fig. 5) where the 20-year maximum tends to be overestimated. The satisfactory simulation of rainfall distribution at several sites suggests that a type-dependent gamma distribution is an adequate model for the non-zero daily rain accumulations across the island. It is noteworthy that all percentiles of the marginal distribution of rain accumulation are properly reproduced in simulations, which suggests that our model is able to simulate the whole spectrum of daily precipitation, from dry days to intense rainfall.

3.4 Simulation of island-scale rain fields

Figure 6 displays the results of the cross-validation procedure focusing on island-scale features. Figure 6a compares observed and simulated spatial patterns for five quantiles of daily rain accumulation across the island of Oʻahu. Results show very good model performance in reproducing the spatial patterns of daily rainfall. This result was expected because the use of empirical copulas combined with rain typing is almost equivalent to resampling the observed spatial patterns conditional to meteorological covariates. However, satisfactory simulation results ensure that the rain-type-based resampling of latent fields is unbiased and that the choice and calibration of the meta-Gaussian model are relevant for the study island.
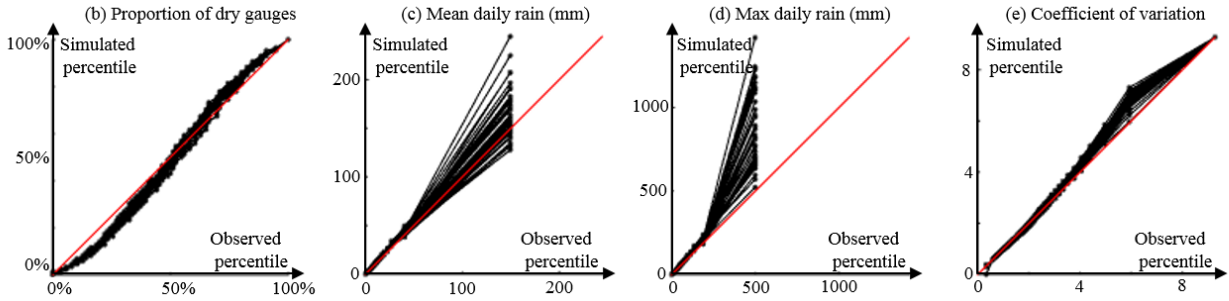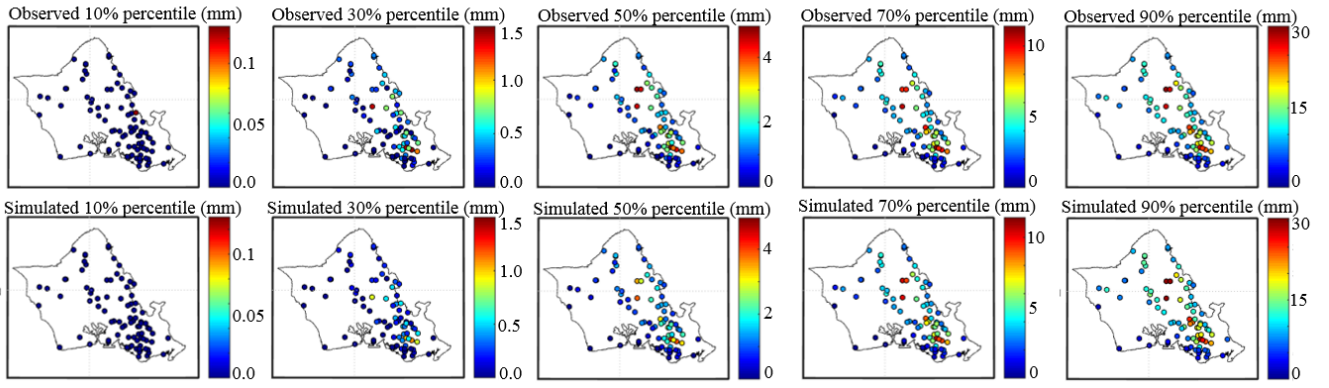
Figure 6: Assessment of island-scale statistics simulation in Oʻahu. (a) Spatial patterns of observed (upper row) and simulated (lower row) percentiles of daily rain accumulation. From left to right: 10%, 30%, 50%, 70% and 90% percentiles. (b–d) Q-q plots of key rain statistics aggregated over the whole rain gauge network: (b) proportion of dry gauges; (c–d) mean and max daily rain; (e) coefficient of variation. Corresponding pdfs are displayed in Supplementary material 3. In (b-e) we display q-q plots between one observation time series (abscissa) and 50 simulations (ordinates). Hence, black dots line up vertically in the q-q plots because for each percentile, 50 simulations are compared to a single observation. To distinguish between simulations, quantiles related to the same simulation are connected by a solid black line.

Figure 6b-e assesses the ability of the model to simulate four key rain statistics - the proportion of dry gauges, mean and max of daily rain accumulation, and coefficient of variation of daily rain across the island - aggregated over all rain gauges of the rain monitoring network of Oʻahu. Results show a slight underestimation of the low percentiles of the proportion of dry gauges (Fig. 6b), which corresponds to a slight overestimation of the frequency of proportions of dry rain gauges below 5% (i.e., 4 gauges over 86 in the present setting). That is, our model tends to simulate rain at all 86 gauges when a very small number of gauges (less than 4) actually records no rain, leading to a slight drizzle effect in space. A careful examination of the spatial patterns of daily rain percentiles (Fig 6a) shows that the patterns of spatial intermittency are properly simulated, which suggests that the drizzle effect is randomly distributed amongst locations, thus reducing its potential impact for applications. This level of accuracy in the simulation of the rain fraction shows that a truncated Gaussian latent field is an appropriate model

for rain intermittency. In addition, the correct simulation of the spatial patterns of dry locations in Fig. 6a suggests that the distance-based modeling of the censored latent values (Eq. 2) coupled with empirical copulas is a proper model for the spatial distribution of dry locations. Similarly, the good agreement between observed and simulated coefficients of variation (Fig. 6e) coupled with the correct simulation of spatial patterns of non-zero daily rain accumulation in Fig. 6a suggest that the selected meta-Gaussian framework captures the spatial distribution of non-zero rain accumulations.

Finally, Fig. 6c-d shows that island-scale daily mean and maximum rain accumulation are properly simulated, despite an overestimation of the last percentile of the maximum, i.e., the 20-year maximum observed over the whole island. This result suggests that the meta-Gaussian framework coupled with the kernel estimation of the transform function parameters performs reasonably well to reproduce the marginal distribution of island-scale rain accumulation. However, the attempt to reproduce both island scale statistics and site-specific marginal distributions (from dry days to heavy rainfall) results in an inaccurate simulation of the island-scale 20-year extreme precipitation. This limitation calls for additional developments before the proposed model can be used for simulating extremes in a spatial context [*Opitz et al.*, 2021].

3.5 Model versatility

To investigate the versatility of our stochastic daily rainfall model, the case study performed in sections 3.1–3.3 for the island of Oʻahu (Hawaiʻi, USA) located in the North Pacific was repeated in supplementary material 4 for the island of Tahiti (French Polynesia) located in the South Pacific. Figure 7 provides a brief overview of the results. This additional cross-validation shows that our model also performs very well for Tahiti, despite a wetter (annual rain reaches 10 000 mm in Tahiti) and more seasonal climate than the Oʻahu case study. In addition, the model adapts automatically to different dataset sizes (86 rain gauges x 21 years for Oʻahu, 26 gauges x 11 years for Tahiti) and rain climatologies due to the selection of different numbers of rain types. These results suggest that our model may be adapted to most high tropical islands across the globe.

466
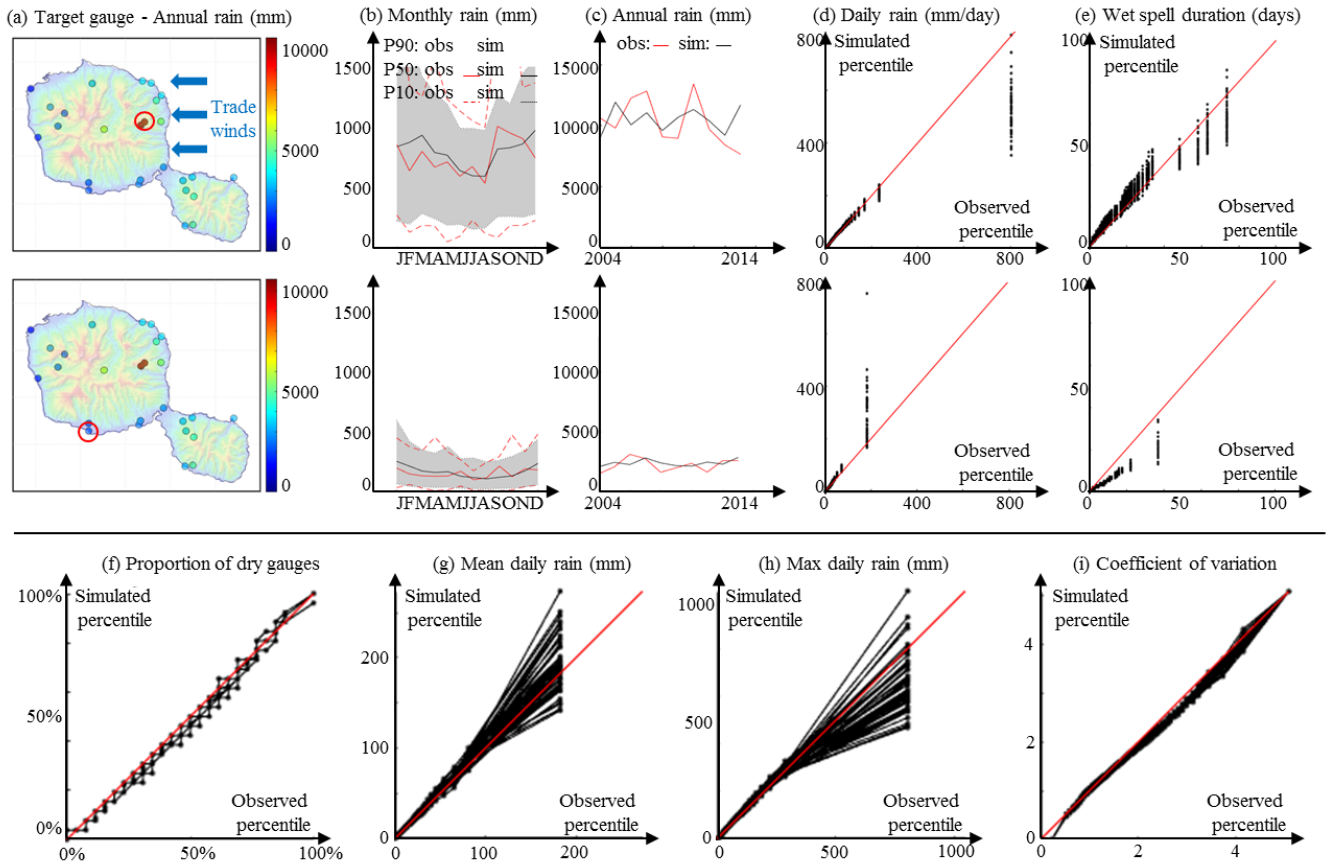
467 **Figure 7: Overview of stochastic daily rainfall simulation for the island of Tahiti, French Polynesia.** (a-e) Site-specific statistics: (a)

468 Target locations. (b) Observed (red) and simulated (black) monthly rain accumulation. (c) Observed (red) and simulated (black) annual rain

469 accumulation. (d) Q-q plot of daily rain percentiles. (e) Q-q plot of wet-spell duration percentiles. (f-i) Island-scale statistics: (f) proportion

470 of dry gauges; (g–h) mean and max daily rain; (i) coefficient of variation.

471

472 **4 Discussion and conclusion**

473 **4.1 Discussion: stochastic modeling of orographic rainfall patterns**

474   Validation results in section 3 show that the proposed model is able to simulate realistic multi-site rainfall time series,

475 which accurately reproduce site-specific and island-scale daily rain statistics for two different tropical islands. This has been

476 made possible by a two-step modeling approach (rain typing and meta-Gaussian representation of island-scale daily rainfall),

477 which takes into account our conceptual knowledge about orographic rain enhancement in tropical islands.

478   The first component consists of rain types, which summarize island-scale rain statistics. Unlike weather type based

479 approaches [*Ailliot et al.*, 2015] [*Réchou et al.*, 2019], we define rain types based on rain features only, i.e., no information

480 about meteorological covariates or large-scale circulation are included during the classification step. This leads to a
481 classification centered on rainfall intensity and spatial distribution, which allows us to explore how island-scale rainfall
482 variability is impacted by orographic effects (section 3.1). The links between rain types and local climate are established in a
483 second step by conditioning the non-homogeneous Markov model of rain type occurrence to meteorological covariates. We
484 conceptualize rain types as the main modes of island-scale daily rainfall variability, which is assumed to be primarily
485 influenced by orographic effects caused by interactions between changing atmospheric conditions and fixed island topography.
486 In this context, one interesting contribution of this study is the refinement of the meteorological predictors proposed by
487 [*Sanfilippo*, 2020] for rain type occurrence in a tropical marine climate, in particular, to distinguish between shallow convection
488 occurring during typical trade wind situations and deeper convection in the vicinity of atmospheric disturbances.

489 The second component of the model consists of a meta-Gaussian representation of island-scale daily rainfall. By
490 explicitly separating rain intensity and spatial distribution, this representation contributed to the performance of the rain typing
491 procedure detailed above and in the identification of rain types with well-defined spatial patterns. When used for stochastic
492 rainfall generation, the adopted meta-Gaussian representation performed well in simulating site-specific rain statistics as well
493 as island-scale spatial patterns of daily rain accumulation. This good performance can be explained by two factors. First, the
494 determination of the censored latent values based on the distance to the closest wet gauge (Eq. 2) generates realistic spatial
495 patterns of dry areas and dry-wet transition [*Schleiss et al.*, 2014]. This contributes to the proper modeling of the spatial
496 intermittency of daily rain fields in tropical islands, which is caused by the drying effect of sinking air masses after crossing
497 mountains. The second innovation of the model is the joint use of empirical copulas and a parametric transform function to
498 model the spatial patterns of non-zero rain. It has the advantage of faithfully preserving the spatial rainfall patterns while
499 generating unobserved values through the kernel density estimation of the transform function parameters distribution. The
500 choice of mimicking the observed spatial rainfall patterns as closely as possible is justified by the complexity of orographic
501 effects and associated rain gradients in tropical islands [*Giambelluca et al.*, 2013] [*Laurent et al.*, 2019] [*Benoit et al.*, 2021].

502 **4.2 Concluding remarks**

503 In this paper we presented a new stochastic daily rainfall generator dedicated to high tropical islands. The combination
504 of (i) rain types, (ii) a non-homogeneous Markov model of rain type occurrence conditioned to meteorological covariates, and
505 (iii) a meta-Gaussian representation of the spatial distribution of daily rainfall allowed us to generate realistic daily rain fields
506 honoring both site-specific and island-scale rain statistics. The performance of the model was carefully tested and illustrated
507 for the islands of Oʻahu (Hawaiʻi, USA) and Tahiti (French Polynesia), both located in the tropical Pacific. Cross-validation
508 results prove the ability of the model to capture and simulate the main features of daily rainfall over these two high tropical
509 islands.

510 The main strength of our model is its ability to simulate diverse patterns of multi-site daily rainfall, as well as their
511 linkage with regional atmospheric conditions. It represents a new tool for stochastic investigation and modeling of orographic
512 rain enhancement on tropical islands with complex topography. The main limitations, however, are (i) the inaccurate

513 simulation of extreme rainfalls, which calls for caution when using our model for flood risk assessment, and (ii) the restriction
514 to multi-site simulation, which calls for an additional step of stochastic interpolation of the multi-site patterns when gridded
515 outputs are required.

516 Because of the above strengths and limitations, the main envisioned applications relate to impact studies that require
517 detailed knowledge of daily precipitation in tropical islands, in particular, when the spatial pattern of rainfall plays an important
518 role. This includes watershed water resources management and eco-hydrological studies.

519 Our model can also be used for the stochastic downscaling of future precipitation projections and thereby contribute
520 to the current efforts to better understand, manage, and secure tropical island water resources in a changing climate. An
521 essential future investigation in this direction will be to assess how well GCMs simulate the set of meteorological covariates
522 we selected to drive our stochastic rainfall generator, in particular the vertical temperature gradient used to inform shallow
523 convection.

524
525

526 *Code and data availability.*

527 The implementation of the proposed stochastic rainfall model is open source (MATLAB implementation) and freely available
528 in the following repository (https://github.com/LionelBenoit/StochasticRainfallGenerator_TropicalIslands). The dataset of
529 daily rainfall observations on O‘ahu is open data and freely available on the Hawai‘i Climate Data Portal
530 (https://www.hawaii.edu/climate-data-portal/data-portal/). An extract of this dataset is available in MATLAB format as a code
531 demo in the same repository as the source code of the model. The dataset of daily rainfall observations on Tahiti is available
532 upon request from Météo France (contact.polynesie-francaise@meteo.fr) and Groupement d'Etudes et de Gestion du Domaine
533 Public de Polynésie Française (secretariat@equipement.gov.pf).

534 *Author contributions.*

535 LB, LS and TWG designed the experiment. MPL and LS compiled the daily rainfall datasets of O‘ahu and Tahiti respectively.
536 LB and ADN selected the meteorological covariates and designed the non-homogeneous Markov Chain. LB and MPL designed
537 the meta-Gaussian model and the rain typing method. LB implemented the model and performed the numerical experiments.
538 LB wrote the paper with input and corrections from all co-authors.

Acknowledgments.

The work of Lionel Benoit is funded by the Swiss National Science Foundation (SNSF), grant number P2LAP2_191395. The work of Lydie Sichoix is supported by the Government of French Polynesia - Ministère de la Recherche through the project E-CRQEST, grant number 05832 MED 08/26/2019. The authors are grateful to the Hawai'i Climate Data Portal for providing the daily rainfall dataset of the island of O'ahu, and to the French Weather Agency (Direction Interrégionale en Polynésie française - Météo France) and the Polynesian public service named Direction de l'Equipement (Groupement d'Etudes et de Gestion du Domaine Public de Polynésie Française - GEGDP) for providing the daily rainfall dataset of the island of Tahiti. The authors are grateful to May Izumy from the Publication services of the School of Ocean and Earth Science and Technology, University of Hawai'i for proofreading this manuscript.

References

Ailliot, P., C. Thompson, and P. Thomson (2009), Space–time modelling of precipitation by using a hidden Markov model and censored Gaussian distributions, *Applied Statistics*, *58*, 405-426, doi:10.1111/j.1467-9876.2008.00654.x

Ailliot, P., D. Allard, V. Monbet, and P. Naveau (2015), Stochastic weather generators: an overview of weather type models, Journal de la Société Française de Statistiques, 156(1), 101-113, ISSN: 2102-6238

Akana, C. L., and K. Gonzalez (2015), Hanau ka Ua Hawaiian Rain Names, 327 pp., Kamehameha Publishing, ISBN13:9780873362467

Allard, D., and M. Bourotte (2015), Disaggregating daily precipitations into hourly values with a transformed censored latent Gaussian process, Stochastic Environmental Research and Risk Assessment, 29, 453-462, doi:10.1007/s00477-014-0913-4

Ambrosino, C., R. E. Chandler, and M. C. Todd (2014), Rainfall-derived growing season characteristics for agricultural impact assessments in South Africa, Theoretical and applied climatology, 115, 411-426, doi: 10.1007/s00704-013-0896-y

Bárdossy, A., and E. J. Plate (1991), Modelling daily rainfall using a semi-Markov representation of circulation pattern occurence, Journal of Hydrology, 122, 33-47, doi:10.1016/0022-1694(91)90170-M

Bárdossy, A., and G. G. S. Pegram (2009), Copula based multisite model for daily precipitation simulation, Hydrology and Earth System Sciences, 13, 2299-2314, doi:10.5194/hess-13-2299-2009

Bauer, P., A. Thorpe, and G. Brunet (2015), The quiet revolution of numerical weather prediction, Nature, 525, 47-55, doi: 10.1038/nature14956

Bennett, B., M. Thyer, M. Leonard, M. Lambert, and B. C. Bates (2018), A comprehensive and systematic evaluation framework for a parsimonious daily rainfall field model, Journal of Hydrology, 556, 1123-1138, doi: 10.1016/j.jhydrol.2016.12.043

Baxevani, A., and J. Lennartsson (2015), A spatiotemporal precipitation generator based on a censored latent Gaussian field, Water Resources Research, 51, 4338-4358, doi:10.1002/2014WR016455

571 Benoit, L., D. Allard, and G. Mariethoz (2018a), Stochastic Rainfall Modeling at Sub-kilometer Scale, *Water Resources*
572   *Research*, *54*, 4108-4130, doi:10.1029/2018WR022817

573 Benoit, L., M. Vrac, and G. Mariethoz (2018b), Dealing with non-stationarity in sub-daily stochastic rainfall models,
574   Hydrology and Earth System Sciences, 22, 5919–5933, doi:10.5194/hess-22-5919-2018

575 Benoit, L., M. Vrac, and G. Mariethoz (2020), Nonstationary stochastic rain type generation: accounting for climate drivers,
576   Hydrology and Earth System Sciences, 24, 1-14, doi:10.5194/hess-24-2841-2020

577 Benoit, L., M. Lucas, H. Tseng, Y.-F. Huang, Y.-P. Tsang, A. D. Nugent, T. W. Giambelluca, and G. Mariethoz (2021), High
578   Space-Time Resolution Observation of Extreme Orographic Rain Gradients in a Pacific Island Catchment, Frontiers
579   in Earth Sciences, 8, 546246, doi: 10.3389/feart.2020.546246

580 Breinl, K., G. Di Baldassarre, M. Girons Lopez, M. Hagenlocher, G. Vico, and A. Rutgersson (2017), Can weather generation
581   capture precipitation patterns across different climates, spatial scales and under data scarcity? Scientific reports, 7,
582   5449, doi:10.1038/s41598-017-05822-y

583 Brown, J. R., M. Lengaigne, B. R. Lintner, M. J. Widlansky, K. van der Wiel, C. Dutheil, B. K. Linsley, A. J. Matthew, and J.
584   Renwick (2020), South Pacific Convergence Zone dynamics, variability and impacts in a changing climate, Nature
585   Reviews Earth and Environment 1, 530-543, doi:10.1038/s43017-020-0078-2

586 Cappelaere, B., et al. (2020), Modeling Land Surface Fluxes from Uncertain Rainfall: A Case Study in the Sahel with Field-
587   Driven Stochastic Rainfields, Atmosphere, 11, 465, doi:10.3390/atmos11050465

588 Caruso, S. J., and S. Businger (2006), Subtropical Cyclogenesis over the Central North Pacific, Weather and forecasting, 21,
589   193-205, doi:10.1175/WAF914.1

590 Caseri, A., P. Javelle, M. H. Ramos, and E. Leblois (2016), Generating precipitation ensembles for flood alert and risk
591   management, Journal of Flood Risk Management, 9, 402-415, doi:10.1111/jfr3.12203

592 Chandler, R. E. (2020), Multisite, multivariate weather generation based on generalized linear models, Environmental
593   Modelling & Software, 134, 104867, doi:10.1016/j.envsoft.2020.104867

594 Daly, C., M. E. Slater, J. A. Roberti, S. H. Laseter, and L. W. Swift (2017), High-resolution precipitation mapping in a
595   mountainous watershed: ground truth for evaluating uncertainty in a national precipitation dataset, International
596   Journal of Climatology, 37, 124-137, doi:10.1002/joc.4986

597 Elison Timm, O., T. W. Giambelluca, and H. F. Diaz (2014), Statistical downscaling of rainfall changes in Hawaiʻi based on
598   the CMIP5 global model projections, Journal of Geophysical Research: Atmospheres, 120, 92-112,
599   doi:10.1002/2014JD022059

600 Foresti, L., and A. Pozdnoukhov (2012), Exploration of alpine orographic precipitation patterns with radar image processing
601   and clustering techniques, Meteorological applications, 19, 407-419, doi:10.1002/met.272

602 Fraley, C., and A. E. Raftery (2002), Model-Based Clustering, Discriminant Analysis, and Density Estimation, Journal of the
603   American Statistical Association, 97(458), 611-631, doi:10.1198/016214502760047131

Frazier, A. G., O. E. Timm, T. W. Giambelluca, and H. F. Diaz (2018), The influence of ENSO, PDO and PNA on secular rainfall variations in Hawaiʻi, Climate Dynamics, 51, 2127-2140, doi:10.1007/s00382-017-4003-4

Gabellani, S., G. Boni, L. Ferraris, J. Von Hardenberg, and A. Provenzale (2007), Propagation of uncertainty from rainfall to runoff: A case study with a stochastic rainfall generator, Advances in Water Resources, 30, 2061-2071, doi:10.1016/j.advwatres.2006.11.015

Gangopadhyay, S., and M. Clark (2005), Statistical downscaling using K-nearest neighbors, Water Resources Research, 41, W02024, doi:10.1029/2004WR003444

Giambelluca, T. W., Q. Chen, A. G. Frazier, J. P. Price, Y.-L. Chen, P.-S. Chu, J. K. Eischeid, and D. M. Delparte (2013), Online Rainfall Atlas of Hawai'i, Bulletin of the American Meteorological Society, 94, 313-316, doi:10.1175/BAMS-D-11-00228.1

Greene, A. M., A. W. Robertson, P. Smyth, and S. Triglia (2011), Downscaling projections of Indian monsoon rainfall using a non-homogeneous hidden Markov model, Quarterly Journal of the Royal Meteorological Society, 137, 347-359, doi:10.1002/qj.788

Hersbach, H., et al. (2018), Operational global reanalysis: progress, future directions and synergies with NWP, ERA Rep. Ser. 27, 1-63 pp, doi: 10.21957/tkic6g3wm.

Hopuare, M., M. Guglielmino, and P. Ortega (2018), Interactions between intraseasonal and diurnal variability of precipitation in the South Central Pacific: The case of a small high island, Tahiti, French Polynesia, International Journal of Climatology, 39, 670-686, doi:10.1002/joc.5834

Hopuare, M., M. Pontaud, J.-P. Céron, P. Ortega, and V. Laurent (2015), Climate change, Pacific climate drivers and observed precipitation variability in Tahiti, French Polynesia, Climate Research, 63, 157-170, doi:10.3354/cr01288

Houze, R. A. (2012), Orographic effects on precipitating clouds, Reviews of Geophysics, 50, RG000365, doi:10.1029/2011RG000365

Huang, S. P., S. T. Quek, and K. K. Phoon (2001), Convergence study of the truncated Karhunen–Loeve expansion for simulation of stochastic processes, International Journal for Numerical Methods in Engineering, 52, 1029-1043, doi:10.1002/nme.255

Hughes, J. P., and P. Guttorp (1999), A non-homogeneous hidden Markov model for precipitation occurence, Applied Statistics, 48, 15-30, http://www.jstor.org/stable/2680815

Jha, S. K., G. Mariethoz, J. Evans, M. F. McCabe, and A. Sharma (2014), A space and time scale-dependent nonlinear geostatistical approach for downscaling daily precipitation and temperature, Water Resources Research, 51, 6244-6261, doi: 10.1002/2014WR016729

Kleiber, W., R. W. Katz, and B. Rajagopalan (2012), Daily spatiotemporal precipitation simulation using latent and transformed Gaussian processes, Water Resources Research, 48, doi:10.1029/2011WR011105

Krajewski, W. F., G. Ciach, and E. Habib (2003), An analysis of small-scale rainfall variability in different climatic regimes, Hydrological Sciences Journal, 48, 151-162, doi:10.1623/hysj.48.2.151.44694

638 Lantuéjoul, C. (2002), Geostatistical Simulation: Models and Algorithms, ISBN: 978-3-662-04808-5

639 Laurent, V., K. Maamaatuaiahutapu, I. Brodien, S. Lombardo, M. Tardy, and P. Varney (2019), Atlas climatologique de la
640   Polynésie française, 232 pp., Météo France, Délégation Interrégionale de Polynésie Française, ISBN:9782111551916

641 Leblois, E., and J. D. Creutin (2013), Space-time simulation of intermittent rainfall with prescribed advection field: Adaptation
642   of the turning band method, Water Resources Research, 49, 3375-3387, doi:10.1002/wrcr.20190

643 Longman, R. J., H. F. Diaz, and T. W. Giambelluca (2015), Sustained Increases in Lower-Tropospheric Subsidence over the
644   Central Tropical North Pacific Drive a Decline in High-Elevation Rainfall in Hawaii, Journal of climate, 28, 8743-
645   8759, doi:10.1175/JCLI-D-15-0006.1

646 Longman, R. J., et al. (2018), Compilation of climate data from heterogeneous networks across the Hawaiian Islands, Scientific
647   Data, 5, 180012, doi:10.1038/sdata.2018.12

648 Longman, R. J., O. Elison Timm, T. W. Giambelluca, and L. Kaiser (2021), A 20-Year Analysis of Disturbance-Driven
649   Rainfall on Oʻahu, Hawaiʻi, Monthly Weather Review, 6, 1767-1783, doi:10.1175/MWR-D-20-0287.1

650 Lyons, S. W. (1982), Empirical Orthogonal Function Analysis of Hawaiian Rainfall, Journal of applied meteorology, 21, 1713-
651   1729, doi:10.1175/1520-0450(1982)021<1713:EOFAOH>2.0.CO;2

652 Maraun, D., et al. (2010), Precipitation downscaling under climate change: Recent developments to bridge the gap between
653   dynamical models and the end user, Reviews of Geophysics, 48, doi:10.1029/2009RG000314

654 Marra, F., and E. Morin (2018), Autocorrelation structure of convective rainfall in semiarid-arid climate derived from high-
655   resolution X-Band radar estimates, Atmospheric Research, 200, 126-138, doi:10.1016/j.atmosres.2017.09.020

656 Mavromatis, T., and J. W. Hansen (2001), Interannual variability characteristics and simulated crop response of four stochastic
657   weather generators, Agricultural and Forest Meteorology, 109, 283-296, doi:10.1016/S0168-1923(01)00272-6

658 Mezghani, A., and B. Hingray (2009), A combined downscaling-disaggregation weather generator for stochastic generation
659   of multisite hourly weather variables over complex terrain: Development and multi-scale validation for the Upper
660   Rhone River basin, Journal of Hydrology, 377, 245-260, doi:10.1016/j.jhydrol.2009.08.033

661 Morin, E., T. Ryb, I. Gavrieli, and Y. Enzel (2019), Mean, variance, and trends of Levant precipitation over the past 4500
662   years from reconstructed Dead Sea levels and stochastic modeling, Quaternary Research, 91, 751-767,
663   doi:10.1017/qua.2018.98

664 Nerini, D., N. Besic, I. V. Sideris, U. Germann, and L. Foresti (2017), A non-stationary stochastic ensemble generator for radar
665   rainfall fields based on the short-space Fourier transform, Hydrology and Earth System Sciences, 21, 2777-2797,
666   doi:10.5194/hess-21-2777-2017

667 Niemi, T. J., J. H. A. Guillaume, T. Kokkonen, T. M. T. Hoang, and A. W. Seed (2016), Role of spatial anisotropy in design
668   storm generation: Experiment and interpretation, Water Resources Research, 52, 69-89, doi:10.1002/2015WR017521

669 Opitz, T., D. Allard, and G. Mariethoz (2021), Semi-parametric resampling with extremes, Spatial statistics, 42, 100445,
670   doi:10.1002/2015WR017521

671   Oriani, F., S. Stisen, M. C. Demirel, and G. Mariethoz (2020), Missing Data Imputation for Multisite Rainfall Networks: A
672   Comparison between Geostatistical Interpolation and Pattern-Based Estimation on Different Terrain Types, Journal
673   of Hydrometeorology, 21, 2325-2341, doi:10.1175/JHM-D-19-0220.1

674   Papalexiou, S. M., and F. Serinaldi (2020), Random Fields Simplified: Preserving Marginal Distributions, Correlations, and
675   Intermittency, With Applications From Rainfall to Humidity, Water Resources Research, 56, e2019WR026331,
676   doi:10.1029/2019WR026331

677   Paschalis, A., P. Molnar, S. Fatichi, and P. Burlando (2013), A stochastic model for high-resolution space-time precipitation
678   simulation, Water Resources Research, 49, doi:10.1002/2013WR014437.

679   Paschalis, A., S. Fatichi, P. M. Molnar, P. S., and P. Burlando (2014), On the effects of small scale space–time variability of
680   rainfall on basin flood response, Journal of Hydrology, 514, 313-327, doi:10.1016/j.advwatres.2013.11.006

681   Paulhus, J. L., and M. A. Kohler (1952), Interpolation of missing precipitation records, Monthly Weather Review, 80, 129-
682   133, doi:10.1175/1520-0493(1952)080<0129:IOMPR>2.0.CO;2

683   Peleg, N., C. Skinner, S. Fatichi, and P. Molnar (2020), Temperature effects on the spatial structure of heavy rainfall modify
684   catchment hydro-morphological response, Earth Surface Dynamics, 8, 17-36, doi:10.5194/esurf-8-17-2020

685   Réchou, A., O. Flores, G. Jumaux, V. Duflot, O. Bousquet, C. Pouppeville, and F. Bonnardot (2019), Spatio-temporal
686   variability of rainfall in a high tropical island: Patterns and large-scale drivers in Réunion Island, Quarterly Journal
687   of the Royal Meteorological Society, 145, 893-909, doi:10.1002/qj.3485

688   Richardson, C. W. (1981), Stochastic simulation of daily precipitation, temperature, and solar radiation, Water Resources
689   Research, 17, 182-190, doi:10.1029/WR017i001p00182

690   Rüschendorf, L. (2009), On the distributional transform, Sklar's theorem, and the empirical copula process, Journal of
691   Statistical Planning and Inference, 139, 3921-3927, doi:10.1016/j.jspi.2009.05.030

692   Sanfilippo, K. M. (2020), Predictor selection and model evaluation for future rainfall projection in Hawai'i, 124 pp, University
693   of Hawai'i at Mānoa, Honolulu, http://hdl.handle.net/10125/73340

694   Schleiss, M., S. Chamon, and A. Berne (2014), Nonstationarity in Intermittent Rainfall: The ''Dry Drift'', Journal of
695   Hydrometeorology, 15, 1189-1204, doi:10.1175/JHM-D-13-095.1

696   Schwartz, G. (1978), Estimating the dimension of a model, The Annals of Statistics, 6, 461-464, doi: 10.1214/aos/1176344136

697   Scott, D. W. (1979), On optimal and data-based histograms, Biometrika, 66(3), 605-610, doi:10.1093/biomet/66.3.605

698   Scott, D. W. (2010), Scott's rule, WIREs Computational Statistics, 2, 497-502, doi:10.1002/wics.103

699   Supit, I., C. A. van Diepen, A. J. W. de Wit, J. Wolf, P. Kabat, B. Baruth, and F. Ludwig (2012), Assessing climate change
700   effects on European crop yields using the Crop Growth Monitoring System and a weather generator, Agricultural and
701   Forest Meteorology, 164, 96-111, doi:10.1016/j.agrformet.2012.05.005

702   Volosciuk, C., D. Maraun, M. Vrac, and M. Widmann (2017), A combined statistical bias correction and stochastic
703   downscaling method for precipitation, Hydrology and Earth System Sciences, 21, 1693-1719, doi:10.5194/hess-21-
704   1693-2017

705 Vrac, M., M. Stein, and K. Hayhoe (2007), Statistical downscaling of precipitation through nonhomogeneous stochastic
706   weather typing, Climate Research, 34, 169-184, doi:10.3354/cr00696

707 Vu, T. M., A. K. Mishra, G. Konapala, and D. Liu (2018), Evaluation of multiple stochastic rainfall generators in diverse
708   climatic regions, Stochastic Environmental Research and Risk Assessment, 32, 1337-1353, doi:10.1007/s00477-017-
709   1458-0

710 Wilby, R. L. (1994), Stochastic weather type simulation for regional cliamte change assessment, Water Resources Research,
711   30, 3395-3403, doi:10.1029/94WR01840

712 Wilcox, C., C. Aly, T. Vischel, G. Panthou, J. Blanchet, G. Quantin, and T. Lebel (2021), Stochastorm: A Stochastic Rainfall
713   Simulator for Convective Storms, Journal of Hydrometeorology, 22, 387-404, doi:10.1175/JHM-D-20-0017.1

714 Wilks, D. S., and R. L. Wilby (1999), The weather generation game: a review of stochastic weather models, Progress in
715   Physical Geography, 23, 329-357, doi:10.1177/030913339902300302

716 Yiou, P. (2014), AnaWEGE: a weather generator based on analogues of atmospheric circulation, Geoscientific Model
717   Development, 7, 531-543, doi:10.5194/gmd-7-531-2014